Correlation between morphology and electrochemical behavior of chromium-free conversion coatings for aluminum alloys corrosion protection

Quentin Boyer[a,*], Maria R. Ortega Vega[b], Célia de Fraga Malfatti[b], Sandrine Duluard[a], Florence Ansart[a]

[a] CIRIMAT, Université de Toulouse, CNRS, Université Paul-Sabatier, 118 Route de Narbonne, 31062 Toulouse Cedex 9, France
[b] Corrosion Research Laboratory - LAPEC, Federal University of Rio Grande do Sul - UFRGS, Av. Bento Gonçalves 9500, Block 4, BLDG 43 427, 2nd FL, Porto Alegre, RS, Brazil

ARTICLE INFO

Keywords:
Chromium-free
Conversion coating
Corrosion protection
Interfacial layers
Electrochemical impedance spectroscopy

ABSTRACT

Chromium(III)-based, tungstate-based and cerium(III)-based conversion coatings on AA2024-T3 are compared in terms of morphology and electrochemical behavior. The durability of coatings is studied under neutral salt spray conditions and in a weakly aggressive electrolyte composed of 0.1 mol/L Na_2SO_4 and 10^{-3} mol/L NaCl. The use of both microscopic and electrochemical analyses such as fitting of electrochemical impedance spectroscopy diagrams allows one to have a better insight into the influence of the interfacial and conversion layers on the degradation phenomena. The role of the remaining native interfacial oxide layer is particularly highlighted, its resistance being the highest at the beginning of the exposure. The degradation of the barrier effect of this interfacial layer is demonstrated to be closely related to the performances of the conversion layer both in terms of passive protection and a reservoir of corrosion inhibitor. Finally, coupled analyses from EIS fitting and microscopic observations allow one to reach a precise interpretation of the strengths and weak points of such system. This diagnostic is an important step towards the optimization of the chromium-free systems.

1. Introduction

Conversion coatings (CCs) are widely used in the aeronautic field for the protection against corrosion of aluminum alloys [1]. These coatings are based on the conversion of the aluminum alloy surface to replace the native oxide layer by a more protective layer. Due to their specific composition and morphology, CCs can promote paint adhesion and/or provide a barrier effect and self healing properties against aggressive ions [2]. This anticorrosion behavior is generally induced by incorporation of corrosion inhibitors in the coating.

Due to their high durability, chromium based conversion coatings are still largely used to protect aluminum alloys against corrosion. However, REACh regulation prohibits hexavalent chromium based substances due to their high toxicity [3]. One of the alternatives is the use of trivalent chromium replacing hexavalent chromium. Nevertheless, in order to avoid the problem related to the use of any chromium species, and especially to their possible transformation in Cr(VI) some authors are working on the elaboration of chromium free conversion systems based on other corrosion inhibitors e.g. cerium [1,4 10], lanthanum [4,11], phosphate [1,12 14], molybdate [1,11,15,16] or tungstate [17,18].

In this paper, a trivalent chromium coating based on a patented protocol [19] and two chromium free conversion systems, tungstate based and cerium based conversion coatings, are investigated. Tungsten and cerium were chosen due to their similar stable oxidation states as compared to chromium. Indeed tungsten transition metal is in the same d block and 6 group in the periodic table as chromium, and presents the same stable oxidation states +III and +VI. WO_4^{2-} tungstate ion presents a low toxicity towards aquatic species [20] and is recognized for its inhibitive corrosion properties in aqueous medium [13]. For example, adsorption phenomenon of WO_4^{2-} anions at flaws and pits is reported [20]. The second conversion system is based on cerium. This ion from lanthanides group has a $[Xe]4f^15d^16s^2$ electronic structure allowing two stable valence states i.e. +III and +IV [21]. This is due to the low energy difference between the outer valence electrons and the 4f electron [10]. In many works an active effect of cerium ions against corrosion has been demonstrated [4,22,23].

Whereas the understanding of the formation and anticorrosive

* Corresponding author.
E-mail address: boyer@chimie.ups-tlse.fr (Q. Boyer).

mechanisms of chromated conversion coatings are highly reported in the literature [24 28], the works on Cr(III) coatings are less abundant and even less for those on chromium free conversion coatings.

This work aims at understanding the differences of performances observed for Cr(III) based and Ce(III) based or WO_4^{2-} based conversion systems. The electrochemical behavior was carefully studied through electrochemical impedance spectroscopy (EIS), with the help of equivalent electric circuit fitting. EIS technique is classically carried out to study the electrochemical behavior of coatings and especially anticorrosive coatings such as conversion coatings [24,26,29 36]. The resulting diagrams highlight phenomena in the system as layers structure, defects or anticorrosive performances. The detailed interpretation of signals for chromium and Cr free coatings will be discussed in this paper following their morphological changes with a special care on the different interfaces of the system.

2. Material and methods

2.1. Conversion system elaboration

Aluminum alloy 2024 T3 (90.7 94.7% Al, 3.8 4.9% Cu, 1.2 1.8% Mg, 0.3 0.9% Mn, ...) with dimensions $80 \times 53 \times 3\,mm^3$ was used as substrate material. Surface preparation before conversion consisted in a degreasing step with a surfactant rich tripolyphosphate borax solution followed by a deoxidation step with SOCOSURF A1858/A1806 commercial solution. Chromium based conversion coatings called TCC in the following were prepared from a solution based on chromium(III) salt in presence of hexafluorozirconate K_2ZrF_6 (Sigma Aldrich). Chromium(III) salt is replaced by sodium tungstate $Na_2WO_4,2H_2O$ (purity ≥ 99% Sigma Aldrich) or by cerium(III) sulfate $Ce_2(SO_4)_3$ (purity = 97% Sigma Aldrich) for the preparation of tungstate conversion coatings (WCC) and cerium conversion coatings (CeCC) respectively. Conversion coatings were prepared in solution with a concentration range in corrosion inhibitor of 0.001 mol/L 0.040 mol/L, a pH value between 3.8 and 4.8, a duration of 3 to 20 min and at temperature range of 30 50 °C. Then, samples were dried for 10 min at 60 °C and stored one week at room temperature in a protective paper against humidity to preserve samples integrity before analysis.

2.2. Characterizations

Surfaces and cross sections of conversion systems were characterized by a Field Emission Gun Scanning Electron Microscopy (FEG SEM) FEI HELIOS 600i. The cross sections were obtained using the FEG SEM with a Focused Ion Beam (FIB) after protection by carbon and platinum layers. After FIB preparations with a Ga ion beam, for SEM observation a 7 µm large cross section is created. To observe the samples by Transmission Electron Microscopy (TEM) a JEOL JEM 2100F instrument coupled with SDD Brucker EDX analyzer or JEOL JEM ARM200F instrument coupled with CENTURIO X EDX analyzer were used. TEM specimens were prepared by thinning towards 20 nm of thickness with FIB.

2.3. Industrial corrosion test

A Neutral Salt Spray (NSS) test (ASTM B117) was also performed in a salt solution containing 0.5 mol/L of NaCl (3% NaCl) in deionized water. This test leads to a rough evaluation of anticorrosion performances by the number of pits appearing during exposure. This specification corresponds to 168 h of exposure without pits. The procedure set up here was to follow the evolution of the pitting and its propagation by 24 h period. In the case of an excessively corroded sample, it was removed from the NSS.

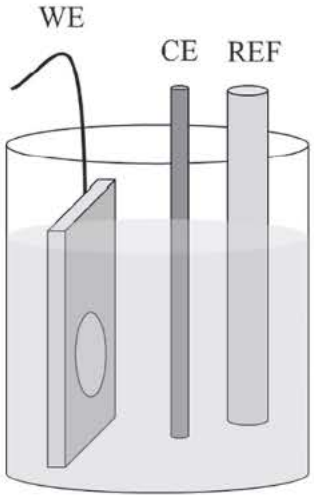

Fig. 1. Cell configuration used for EIS measurements, WE is the working electrode, CE the counter electrode in graphite and REF the saturated calomel reference electrode.

2.4. Electrochemical tests

Electrochemical Impedance Spectroscopy (EIS) measurements were carried out on AA2024 T3 substrate without conversion and on TCC, WCC and CeCC using a PGSTAT30 Potentiostat with Nova software. A three electrode cell was used to perform analyses, with a saturated calomel electrode (SCE) as reference electrode, a graphite rod as counter electrode and a 3 cm in diameter exposed area of working electrode (Area = 7.07 cm^2). Samples were vertically set in the electrolyte solution (Fig. 1). A volume of 230 mL of naturally aerated electrolyte composed of 0.1 mol/L of Na_2SO_4 with 10^{-3} mol/L of NaCl was used. This large volume is favorable for a more homogeneous and durable distribution of aggressive ions compared to other corrosion cells. EIS measurements were recorded from 100 kHz to 10 mHz with 10 points per decade and a sinusoidal amplitude of 14.14 mV (RMS). Open Circuit Potential (OCP) was measured for 20 or 30 min before EIS to check the stability of systems. Three samples were prepared and analyzed by EIS to confirm the good results' reproducibility. Analysis of EIS results requiring equivalent circuits was performed using Zview software. All fitting results were checked by a chi squared factor ($\chi \leq 10^{-4}$).

3. Results and discussion

3.1. Microstructure and composition before exposure

SEM images of TCC, WCC and CeCC surfaces are reported in Fig. 2. The three conversion systems surfaces show a similar morphology composed of homogeneously dispersed grains around 40 50 nm in diameter (see inserts in Fig. 2 b, d and f). A complete coverage of the substrate is observed, even in the more creviced areas. Presence of crevices is mainly due to the deoxidation step that removes intermetallic compounds from the surface.

Cross sections of CCs shown in Fig. 3 give information about thickness and microstructure of conversion systems. A statistic measurement of samples thicknesses exhibits an average value of 110 ± 30 nm, 75 ± 15 nm and 80 ± 15 nm for TCC, WCC and CeCC respectively. These values are in good agreement with the thickness for TCC reported in literature [24,36,37]. The FEG SEM (Fig. 3 a) and TEM (Fig. 3 b) images of TCC validates the existence of a bilayer coating composed of an outer layer and an inner layer with different morphologies and composition. Indeed, EDX analysis in Fig. 4 a reveals that the outer layer presents an important part of Cr and Zr elements

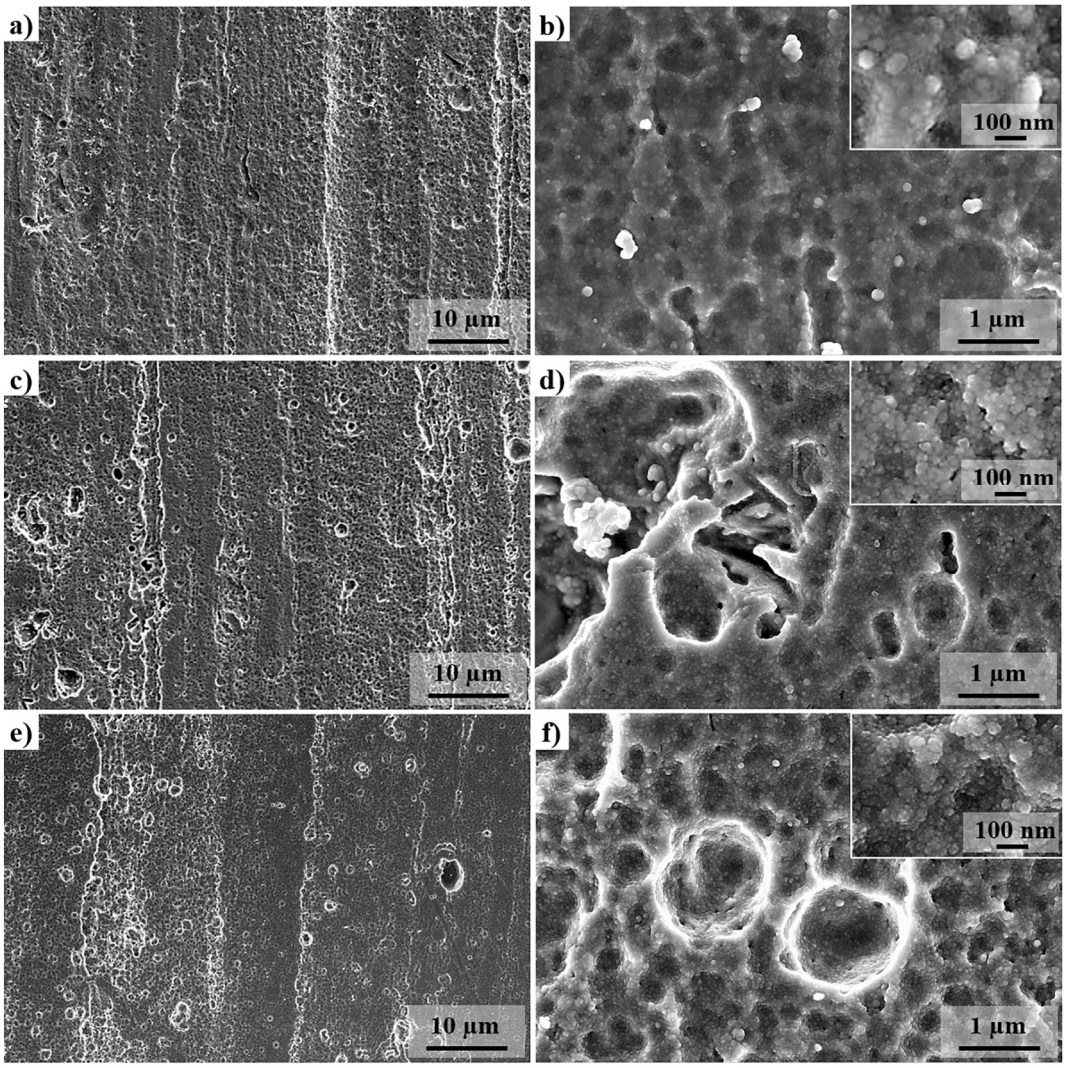

Fig. 2. FEG-SEM top view images of as deposited (a, b) TCC, (c, d) WCC and (e, f) CeCC.

whereas the inner layer is mainly composed of Al and Zr elements. On the other hand, some traces of F and Cu were detected in the coating. These observations are in agreement with the literature on trivalent chromium conversion systems on aluminum alloy 2024 T3 [26,38]. It was already demonstrated that fluorides may be present in the con version system. Indeed, F^- species from conversion solution help to the dissolution of native oxide layer and to the formation of conversion layer [24]. Moreover, the complexed nature of F^- in hexa fluorozirconate reduces the aggressiveness of fluoride and leads to formation of ZrO_2 and K_3AlF_6 components [36,39]. The presence of fluoride in the conversion solution induces both dissolution and re deposition phenomena of copper [25,36].

Concerning WCC (Fig. 3 c and d) and CeCC (Fig. 3 e and f), bi layered coatings are also observed. EDX analysis performed on WCC (Fig. 4 b) shows the presence of Zr, W and Cu elements in the outer layer. The inner layer presents a majority of aluminum oxide with F traces. Finally, it was observed that a thin layer (around 5 nm) between the coating and the substrate corresponds to copper probably from re deposition step.

As already observed by surface and cross section observations, the outer layer morphologies seem to be similar to the one corresponding to TCC for WCC and CeCC. On the contrary, the inner layers are different for the three systems. Whereas TCC presents a continuous inner layer on the whole length of the sample, WCC inner layer is non continuous with defects around 10 20 nm in size (see arrow in Fig. 3 d) and for CeCC the inner layer presents porosity with pores around 5 10 nm in size (see arrows in Fig. 3 f). For both WCC and CeCC, these defects can lead to a rapid diffusion of aggressive species towards the substrate resulting in an accelerated degradation during exposure. Indeed, the literature re ports the reverse effect for chromated conversion coatings, with the continuous and rather dense inner layer playing the role of a barrier layer [32].

Some delamination defects, visible in Fig. 3 c for example, are present between the substrate and the coating for TCC and WCC. This delamination phenomenon was already noticed by Guo et al. and re sults from the dehydration in FIB/SEM and/or TEM vacuum chamber [37].

3.2. *Industrial neutral salt spray test*

The Neutral Salt Spray (NSS) was used to check the performances of the conversion coatings as regards to industrial requirements. This test produces a simple binary result about anticorrosive performances of conversion coatings in 0.5 mol/L chloride concentrated spray. Validation of systems depends on pits presence (according to ASTM B117 standard). In NSS, the TCC resists to pitting around 48 h whereas WCC and CeCC do not resist > 24 h. Thus, TCC shows better macro scopic performance against corrosion after this test compared to the alternative coatings. To understand such different behaviors, exposure in a less aggressive solution (0.1 mol/L of Na_2SO_4 with 10^{-3} mol/L of

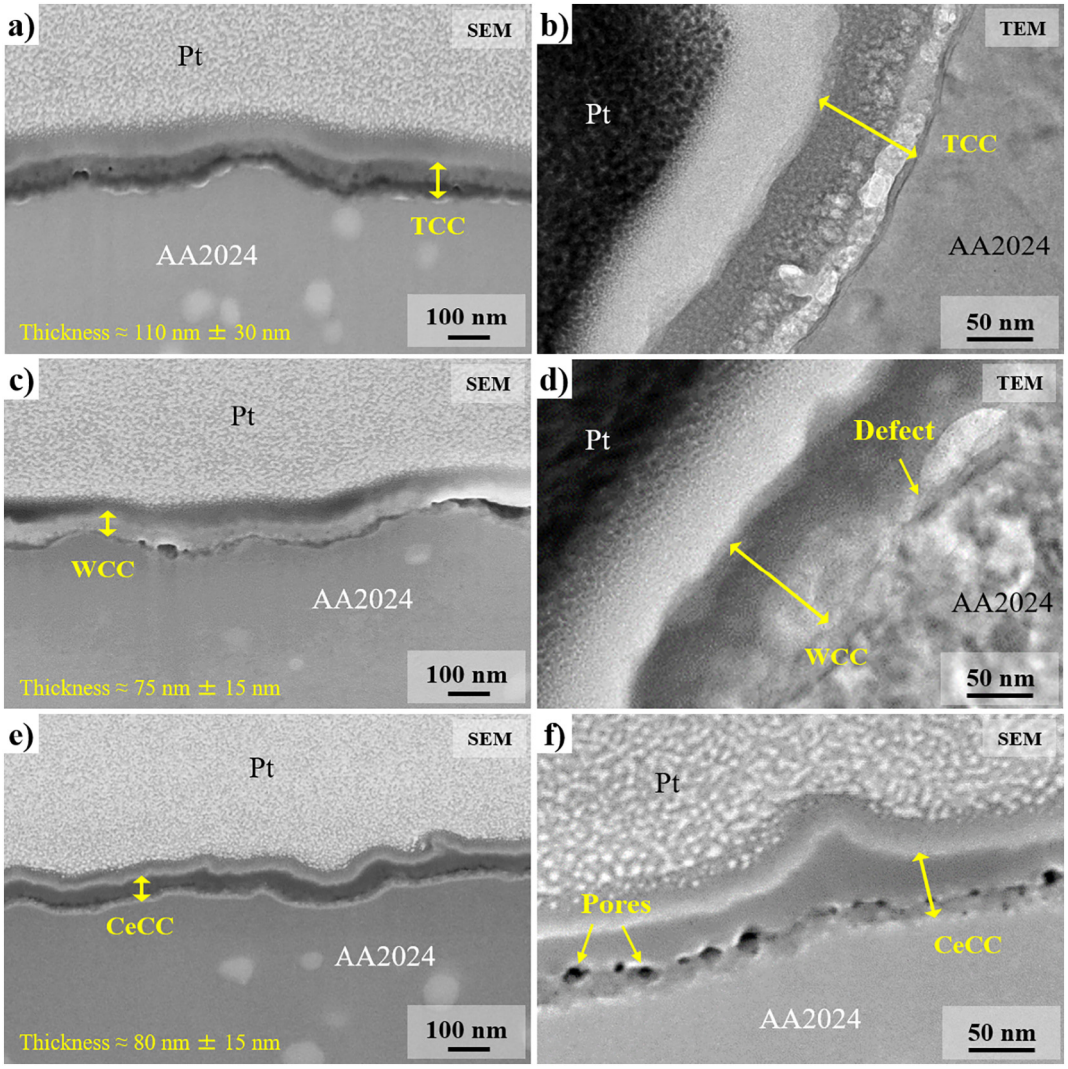

Fig. 3. Micrographs of the cross-sections of as deposited (a, b) TCC, (c, d) WCC and (e, f) CeCC. FEG-SEM cross-sections (a, c, e, f) and TEM slice observations (b, d).

NaCl) was performed. The CC morphology after exposure and electro chemical behavior during exposure will be firstly detailed, and then compared with the chromium free conversion coatings behaviors.

3.3. Microstructure after exposure

Exposure by immersion in a weakly aggressive electrolyte, com posed of 0.1 mol/L of Na_2SO_4 and 10^{-3} mol/L of NaCl, was carried out. These conditions are used to decrease the degradation rate of the conversion coatings in order to facilitate EIS interpretation.

SEM images of TCC surfaces on Fig. 5 a and b, show the appearance of corrosion product clusters. These corrosion products are probably composed of Al(III) and Cr(III) [24]. Indeed, the attack of aluminum alloy by aggressive substances e.g. chloride ions Cl^- leads to releasing of chromium as chromate (CrO_4^{2-}) near the pitting area. A precipita tion in Al(III)/Cr(III) mixed oxide occurs and provides a passive chro mated corrosion product. It was shown that the corrosion product formed in weakly aggressive electrolyte is more compact and presents a more pronounced barrier effect than in aggressive electrolyte as 0.5 mol/L NaCl [32]. WCC is characterized by cracking of the coating for exposure (Fig. 5 c) that leads to corrosion attack of the substrate. Concerning CeCC, the coating is degraded by pitting corrosion as can be seen on Fig. 5 e.

At higher magnification (Fig. 5 b, d, f), the degradation of the coating compactness can be observed for all systems. Nevertheless, even if the surface topography is similar at high magnification, cross section images of the conversion systems help to understand the cor rosion mechanisms (Fig. 6). The exposure in the electrolyte impacts the conversion coating itself. Indeed, after exposure, for the three systems the frontiers between the inner and the outer layers are less pro nounced. Fig. 6 a and b show that the TCC is still present on the whole surface and no pits are observed. Moreover, the thickness of TCC in creases during exposure from 110 ± 30 nm to go to 155 ± 40 nm. This is probably due to the corrosion product formation in the layer and on the top of the layer. On the contrary, WCC and CeCC are slightly thinner after exposure. Thickness are 70 ± 20 nm and 70 ± 10 nm for WCC and CeCC, respectively (75 ± 15 nm and 85 ± 15 nm before exposure).

Cross section images on Fig. 6 c and e point the degradation of the substrate by corrosion process because of the presence of initial defects such as discontinuities or pores in the inner layer. For WCC and CeCC, apart from the pits, the remaining conversion layers are homogeneous, continuous and adherent to the substrate (Fig. 6 d and f). Degradation of chromium free systems might be initiated on the defects of the inner layer which would be the starting point of corrosion phenomena. To better understand conversion system behavior during exposure, EIS analysis and fitting were carried out.

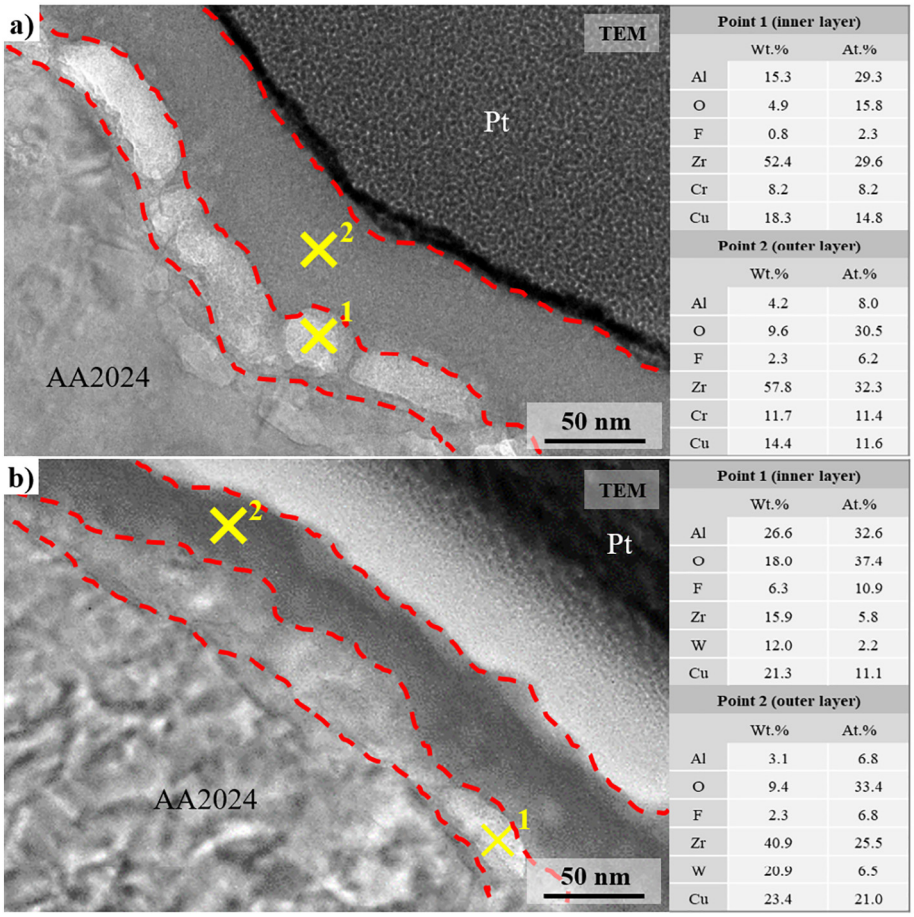

a) Point 1 (inner layer)	Wt.%	At.%
Al	15.3	29.3
O	4.9	15.8
F	0.8	2.3
Zr	52.4	29.6
Cr	8.2	8.2
Cu	18.3	14.8
Point 2 (outer layer)		
	Wt.%	At.%
Al	4.2	8.0
O	9.6	30.5
F	2.3	6.2
Zr	57.8	32.3
Cr	11.7	11.4
Cu	14.4	11.6

b) Point 1 (inner layer)	Wt.%	At.%
Al	26.6	32.6
O	18.0	37.4
F	6.3	10.9
Zr	15.9	5.8
W	12.0	2.2
Cu	21.3	11.1
Point 2 (outer layer)		
	Wt.%	At.%
Al	3.1	6.8
O	9.4	33.4
F	2.3	6.8
Zr	40.9	25.5
W	20.9	6.5
Cu	23.4	21.0

Fig. 4. EDX analyses of (a) TCC and (b) WCC on TEM slice.

3.4. Electrochemical behavior

Anticorrosion performance of conversion systems was evaluated by EIS. As stated before, the use of a low concentrated NaCl solution re duces the degradation processes kinetics for a better understanding of the electrochemical behavior. Moreover, due to the use of SO_4^{2-} ions it is easier to study passive layers and pitting corrosion on Cu rich alu minum alloy [32,40]. This is why a weakly aggressive solution of 0.1 mol/L of Na_2SO_4 with 10^{-3} mol/L of NaCl was used as electrolyte. TCC, WCC and CeCC were exposed up to 245 h in the electrolyte. Open Circuit Potential (OCP) measurements were recorded during 30 min before each EIS measurement. OCP graphs are presented in Fig. 7 a, c and e and show the evolution of the systems stability. EIS measure ments were made after OCP at $t_{0+30min}$, t_{0+5h}, t_{0+24h}, t_{0+48h}, t_{0+96h} and t_{0+245h} from the beginning of the immersion. The evolution of Bode diagrams is presented in Fig. 7 b, d and f.

The OCP of TCC remains in the range of order of the final potential value around −0.40 V/SCE. The equilibrium of the system is reached in the first minutes after immersion and its evolution is stable during ex posure. This is well correlated with microscopic observations provided that such products are protective (non presence of pits and cracks). This hypothesis will be checked after EIS analysis.

On the opposite, there is a large decrease of OCP values for WCC and CeCC. Although both systems have a higher OCP than TCC (around −0.20 V/SCE for WCC, CeCC versus −0.40 V/SCE for TCC), even for short times of exposure, this voltage decreases constantly in the elec trolyte. It could mean that there is an uncompensated degradation phenomenon due to the aggressive ions of electrolyte solution. It can be related to the defects in the coatings as a non continuous inner layer or porosities in the WCC and CeCC coatings respectively. The final OCP value is towards −0.43 V/SCE.

Bode diagrams presented on Fig. 7 b, d and f exhibit the im pedance modulus and phase evolution throughout exposure. Impedance modulus at the lowest frequency (10^{-2} Hz) represents the global re sistance of the conversion systems. At $t_{0+30min}$, the three systems pre sent a global resistance close to $3 \times 10^6\ \Omega{\cdot}cm^2$ that means that global anti corrosive properties are similar at the very beginning of the ex posure. Moreover, the global trend for the resistance evolution versus time is the same for the three systems with a sharp decrease with ex posure time. However, the degradation is slower and less marked for TCC, the global resistance remaining higher than $10^5\ \Omega{\cdot}cm^2$ after 245 h. On the contrary, the WCC global resistance drops down to $3 \times 10^4\ \Omega{\cdot}cm^2$ after 245 h despite a slower decrease in the first im mersion times as compared to CeCC. The global resistance for CeCC quickly decreases at the beginning of the immersion then stabilizes; the global resistance evolution is negligible after 24 h and remains in the $10^5\ \Omega{\cdot}cm^2$ order of magnitude.

On Fig. 7 b, TCC phase diagram shows several time constants: one at low frequency, one at high frequencies (around 10^3 Hz). Similar Bode diagrams have already been obtained in the literature for similar con version coatings [29,31,34,36,41]. The time constant at high fre quencies (HF) is referenced by authors as resistive and capacitive re sponses of the pores and defects in conversion coatings [24,32]. Another one at low frequencies (LF) that is attributed to the charge transfer reaction in the literature dealing with Trivalent Chromium process (TCP) [24,26,34,36,42]. However, this time constant could also be relative to the native oxide layer given the easiness of formation of oxides on aluminum alloys in air or any oxidative media. This alter native hypothesis is largely developed in the literature for other type of coatings on aluminum alloys [43 46]. The conclusions of this work will

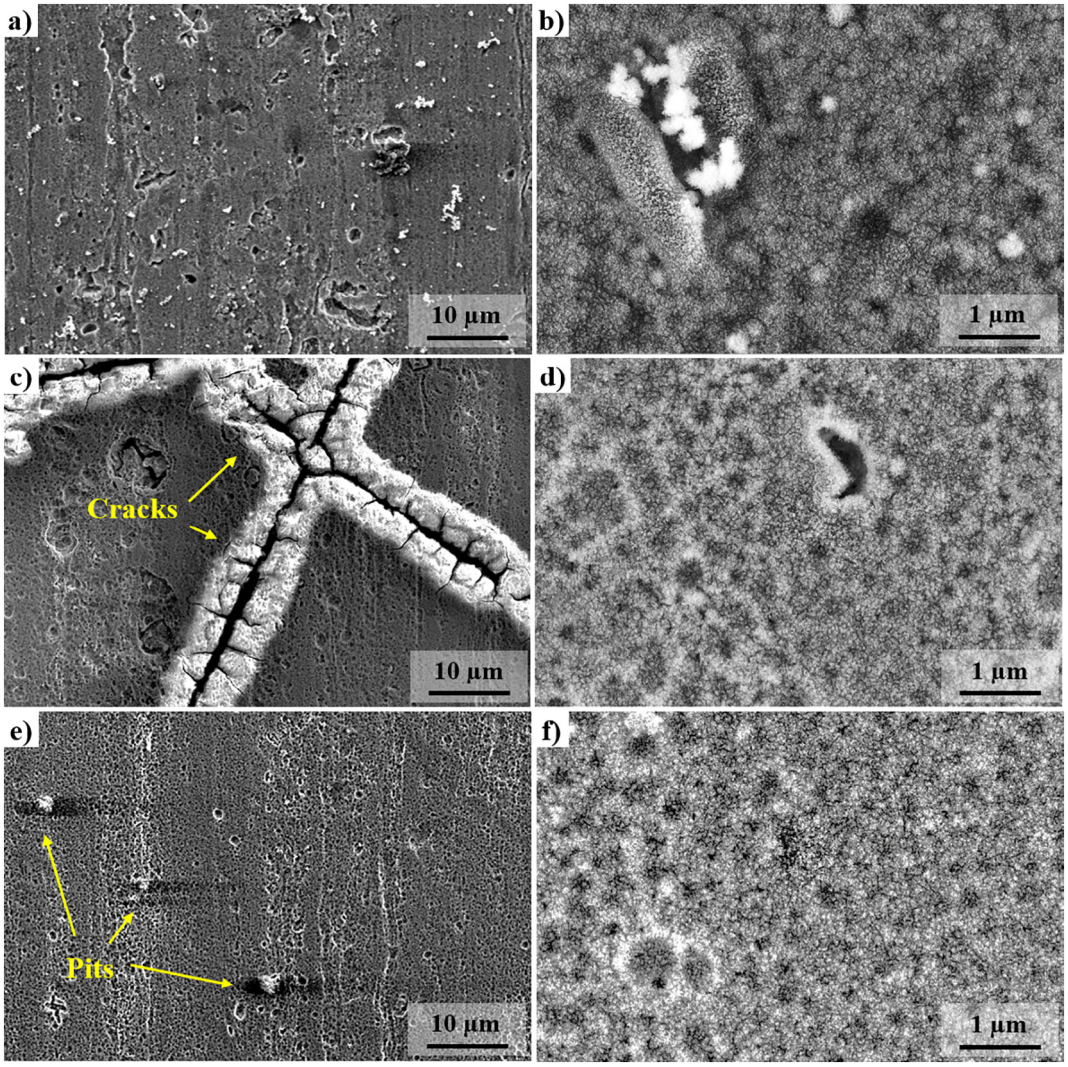

Fig. 5. FEG-SEM top view images of (a, b) TCC, (c, d) WCC and (e, f) CeCC after 245 h of exposure in 0.1 mol/L of Na_2SO_4 with 10^{-3} mol/L of NaCl.

drive the interpretation towards the presence of the interfacial native oxide layer under TCC and chromium free conversion coatings. To our knowledge it is the first time that the presence of the native oxide layer (formed after surface preparation and partially dissolved during the conversion) is demonstrated for such systems. The impedance and morphological analyses to support this interpretation will be detailed in the following. In particular EIS diagram equivalent circuit fitting was performed to more precisely comprehend the systems.

WCC and CeCC present a different behavior. First, the signal at HF representative of the conversion layer at $t_{0+30min}$ is less visible than for TCCs; it denotes a lower barrier effect of the conversion coating. Moreover, a strong drop of phase shift at LF, more particularly for CeCC, appears during exposure. It can be related to the CeCC coatings lower thicknesses as compared to TCC (80 ± 15 nm vs 110 ± 30 nm for TCC) and its porous character (Fig. 3). The interfacial layer as similated to native oxide is quickly reached by aggressive Cl^- ions leading to a rapid degradation of the films and corrosion of the sub strate.

The smaller defects of CeCC as compared to WCC (porosities versus absence of the inner layer) could explain the higher global resistance of CeCC. Observations of the systems morphology after exposure in the weakly aggressive electrolyte gave ~~away~~ some information about the evolution of chromium free systems. WCC was degraded because of the cracking of the coating whereas CeCC endured pitting corrosion. EIS spectra fitting with equivalent circuits will be detailed in the next paragraph to better understand these phenomena.

3.5. Equivalent electrical circuits

To help to identify the different electrochemical processes that take place at the conversion systems (conversion coating and alloy) during exposure, equivalent circuits fitting was performed. Many equivalent circuits have been proposed in the literature in accordance with TCC, WCC and CeCC behavior [24,29 34,36,41]. Here, three circuits have been selected and are presented in Fig. 8 after trials and errors with the aforementioned criteria (chi squared factor lower than 10^{-4}). All the RC elements present in these circuits are composed of a resistance R and a constant phase element (CPE) as non ideal capacitor with impedance Z_{CPE} expressed in Eq. (1):

$$Z_{CPE}(\omega) = 1/Q(j\omega)^n \quad (1)$$

This impedance depends on ω the angular frequency, Q the effective CPE parameter and n the intensity of deviation from an ideal system. Indeed, several authors demonstrated the interest of using of CPE to take into account the heterogeneities, i.e. porosity or defects, in systems [30]. TCC impedance results were fitted by two different equivalent circuits according to immersion times: circuit a) (Fig. 8 a) from t_{0+5h} to t_{0+48h}, then circuit b) (Fig. 8 b) until the end of the experiment. Indeed, due to non stability of the results during the first minutes of immersion in electrolyte, EIS fitting results at $t_{0+30min}$ are not presented here, for

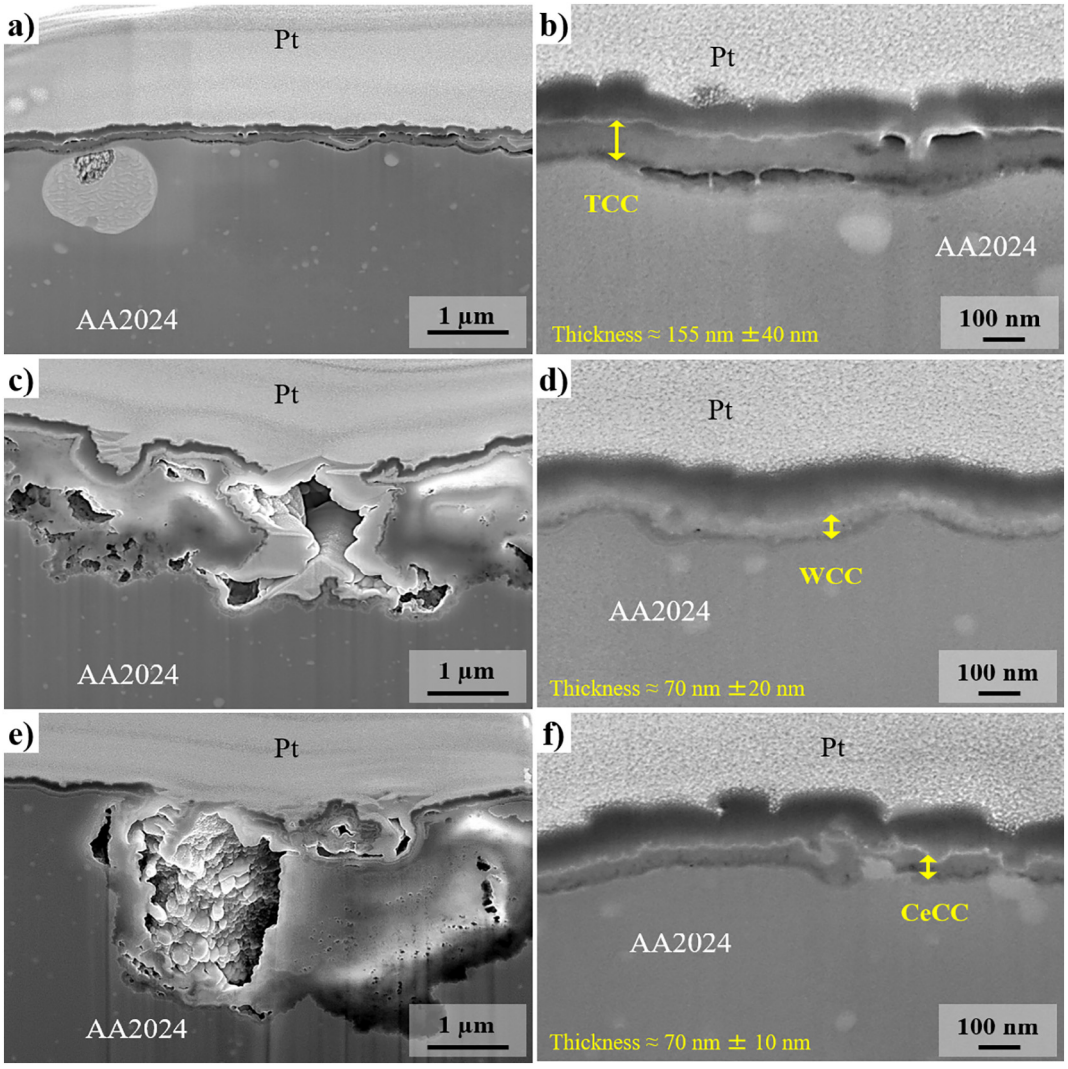

Fig. 6. FEG-SEM cross-sections of (a, b) TCC, (c, d) WCC and (e, f) CeCC after 245 h of exposure in 0.1 mol/L of Na_2SO_4 with 10^{-3} mol/L of NaCl.

the same reason the effective capacitance values at this duration could not be calculated.

The circuit a) presented in Fig. 8 a is composed of $R_{electrolyte}$ as the electrolyte solution resistance, two RC elements in parallel and a RC element in series. This circuit is coherent with the morphological in formation. Indeed, the two RC elements in parallel can stand for the outer and inner layers of the conversion coating. The additional RC in series is related to the highest resistances (around $10^6\ \Omega{\cdot}cm^2$) and is similar at the very beginning of the immersion for the three system. This is why it can be interpreted as corresponding to the thin interfacial native oxide layer (1 2 nm) that formed on top of the substrate after the preparation surface treatments and that is not fully dissolved during the conversion treatment [47]. Furthermore, this last RC element was not attributed to the charge transfer resistance and double layer capaci tance but to interfacial native oxide layer due to the effective capaci tance values at the start of exposure. These values are in the range of what is known in the literature for oxide resistances and are too low to be due to charge transfer. Indeed, the hypothesis of the presence of an interfacial layer is confirmed by Table 1 that presents the values of effective capacitance obtained by Eq. (2) [48,49]:

$$C_{eff} = Q^{1/n}R^{(1-n)/n} \quad (2)$$

At the beginning of the immersion, the C_{eff} values of native oxide layer for TCC, WCC and CeCC are in the same range of order as the values reported by some authors for native oxide layer on AA2024 T3 alloy [43,44]. These values remain stable during the first immersion times, and then increase up to one order of magnitude at 96 h for CeCC and at 245 h for TCC and WCC. The transition occurs later for TCC and WCC than for CeCC. At high immersion times the C_{eff} values reach much higher values which could correspond to charge transfer with the alu minum substrate. Indeed, in the literature, the C_{eff} values are between 4 and 7 µF/cm^2 for native oxide layer while they would be superior to 20 µF/cm^2 if the phenomena would be charge transfer [43,44]. These results are in accordance with a higher protection of TCC coatings with a more lasting native oxide layer. Moreover, these results indicate that there is probably a overlapping of phenomena (interfacial oxide layer and charge transfer) during exposure because corrosion process occurs.

Thus at the beginning of exposure, fitting data of TCC with circuit a) allows separating the three phenomena related to the inner layer, outer layer and interfacial oxide layer, two of them being at LF, i.e. TCC inner layer and interfacial oxide layer responses. From t_{0+96h} to t_{0+245h}, circuit a) was not appropriate and the TCC behavior was better fitted by the circuit b) presented in Fig. 8 b. In this case, the RC circuit of the interfacial layer is maintained but a single RC element is sufficient to fit the data from conversion layers behavior. Indeed, the inner and outer layers properties are no longer different enough to be separated. This is in accordance with morphology data and the merging of the two layers (Fig. 6 a, b). On the other hand, another RC subcircuit is to be added in series at medium frequencies. The resistance value of this element is rather high as compared to conversion coating resistance. SEM and

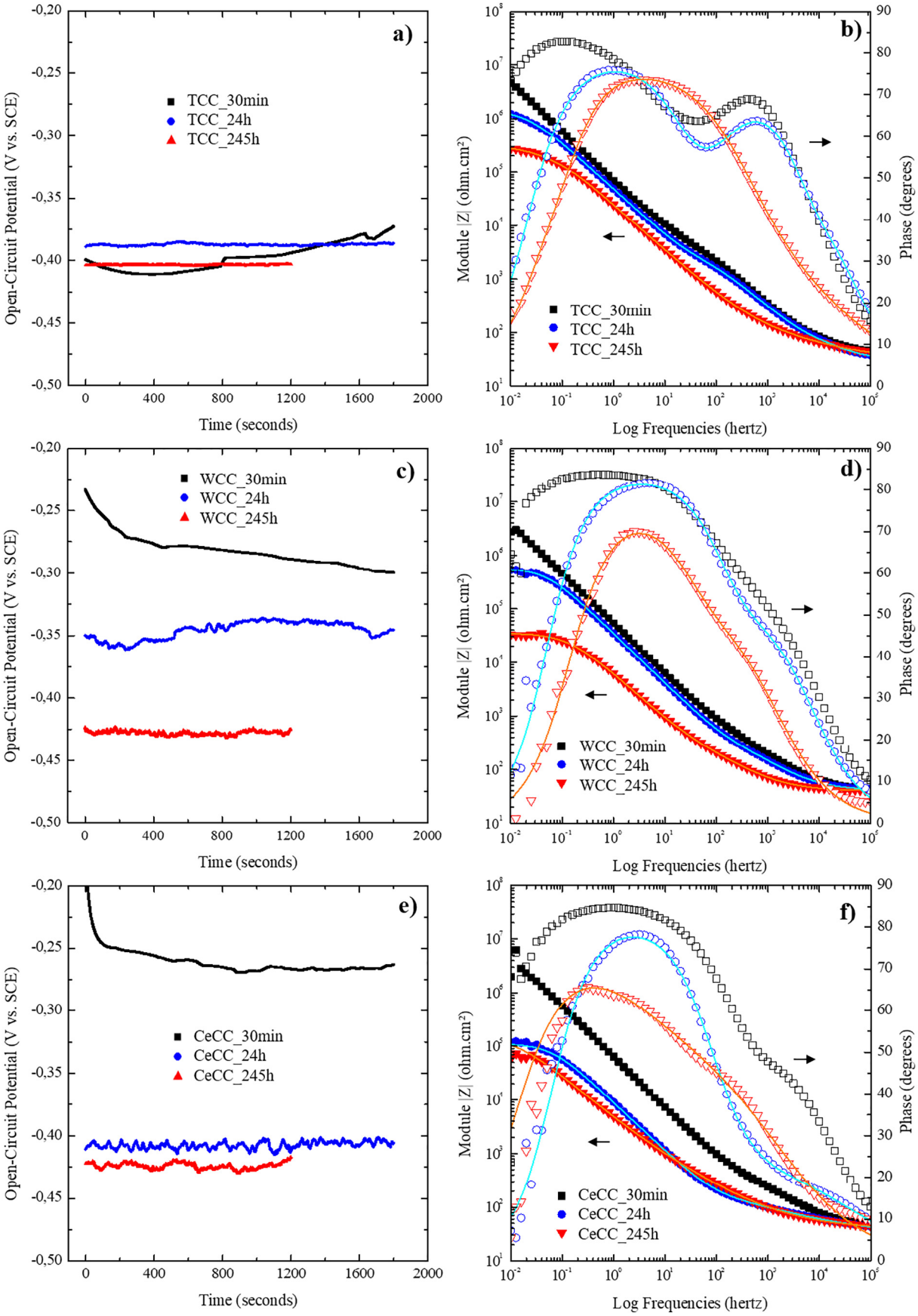

Fig. 7. OCP evolution (a, c, e) and EIS Bode diagrams (c, d, f) for TCC, WCC and CeCC. Fitting results are presented as solid lines on EIS diagrams for t_{0+24h} and t_{0+254h}.

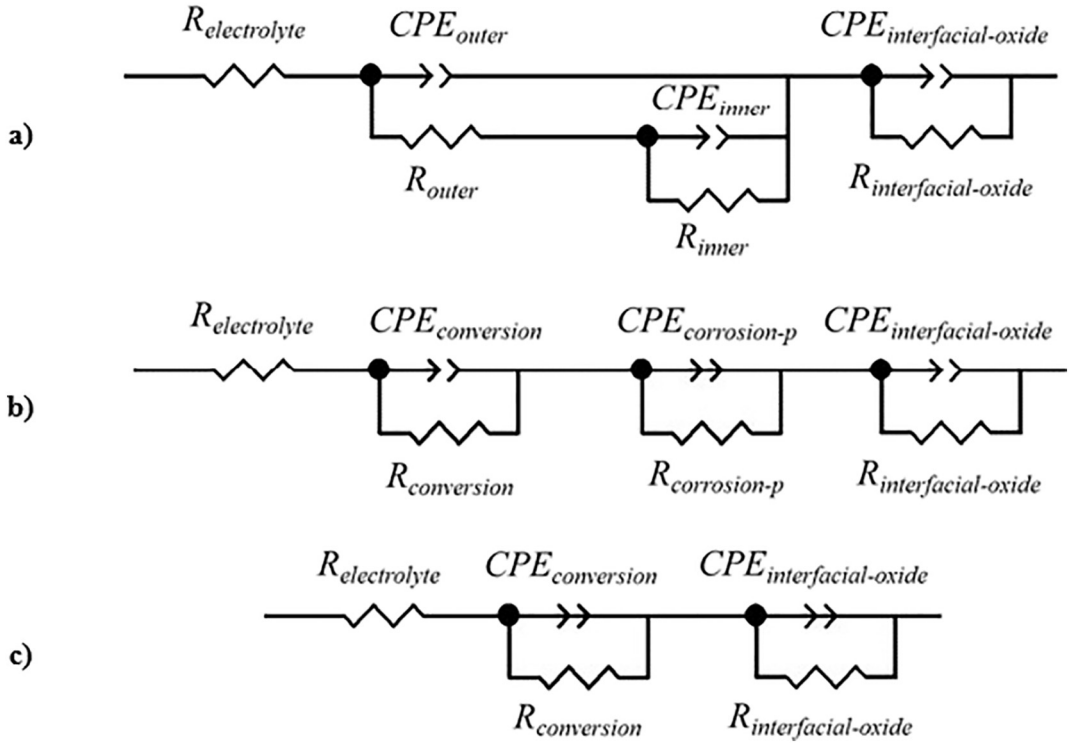

Fig. 8. Equivalent circuits used to fit TCC until 48 h (a), and until 245 h (b) and WCC or CeCC (c).

Table 1
Effective capacitance of native oxide layer on the AA2024 substrate with TCC, WCC and CeCC during exposure.

	Effective capacitance (μF/cm^2)				
	t0 + 5 h	t0 + 24 h	t0 + 48 h	t0 + 96 h	t0 + 245 h
TCC	4.0	3.9	5.3	9.1	23.4
WCC	4.7	5.1	5.7	11.7	33.4
CeCC	3.3	4.6	22.8	41.3	80.6

TEM analysis, where corrosion products are visible on top and in the conversion coating, helped to attribute this new resistance to the pre sence of protective corrosion products forming at the surface or in the conversion layer. This phenomenon is known in the literature especially for TCC, the self healing effect being conferred by chromate stored as CrO_4^{2-} that reduces into $Cr(OH)_3$ and α CrOOH at corroding sites to produce protective corrosion product [24].

Table 2 shows the evolution of the conversion layers, interfacial oxide layer and corrosion products resistances, admittances and *n* parameters extracted from simulation of TCC with circuit a) for im mersions lower than 48 h and circuit b) from 96 h to 245 h. Table 2 makes visible the high resistance of interfacial oxide layer more parti cularly in the first hours of exposure: oxide resistance is in the range of 10^5 10^7 Ω·cm^2 compared to conversion coating resistance around 10^2 10^3 Ω·cm^2. The high *n* value gives information on the hetero geneity of the layers and interfaces [49]. The high *n* value (close to 0.90) indicates that the morphology of the oxide layer is probably homogeneous and dense. The *n* values of outer and inner layers are in very good accordance with the previous observations concerning the differences of porosity in TCC: the outer layer is less dense (and more heterogeneous) with *n* value close to 0.77 against 0.90 for inner layer. Bode diagrams at first time of immersion in Fig. 7 b show phase shift maxima around 70° for outer layer (HF) and around 85° for inner and oxide layers (LF), in agreement with *n* values computations.

After a critical exposure time in electrolyte solution of around 48 h, the slow deterioration of the TCC is emphasized by the decrease of the inner layer resistance, interfacial oxide resistance and *n* values, and by increasing of admittances. This is related to the formation of pores and the concomitant increase of the flux of aggressive ions through the conversion system [36]. A decrease of conversion layer resistance from 425.8 to 154.5 Ω·cm^2 and *n* values from 0.61 to 0.41 is measured for 96 and 245 h of immersion respectively. At the same time, the signal of the corrosion phenomena appears and the corrosion products show higher resistance values (around 4×10^5 Ω·cm^2). As already explained this high corrosion protection is due to the self healing properties of chro mium, with release of Cr(IV) and its use for the formation of protective Cr(III) corrosion products. It yields high resistance and *n* values of corrosion products elements. Indeed, after only 245 h exposure, only one pit is detected and this one is sealed by whitish corrosion product. Finally the very good accordance between the measured and the cal culated curves from the fitting of TCC behavior are shown on Bode diagrams in Fig. 7 b.

WCC and CeCC impedance results were fitted with equivalent cir cuit c) presented in Fig. 8 c. This circuit is less complex than the first two. It is composed by only two RC series elements. This circuit is re levant for WCC and CeCC; it simulates the signal from the outer con version layer and the interfacial oxide layer. It is coherent that the inner layer could not be detected separately from the outer layer due to merging between the both layers. In the same way that TCC, effective capacitances of oxide layers for WCC and CeCC are in accordance with the order of magnitude in the literature for chromium based system ($C_{eff} \approx 4$ 7 μF/cm^2). But, as it is shown in Tables 3 and 4, the trend of both interfacial oxide resistance and outer layer resistance values for these two non chromated conversion systems are quite different. The evolution of oxide resistance and outer conversion layer resistance for WCC seems to be similar to TCC with a constant decrease of oxide re sistance and stable outer conversion coating resistance. On the con trary, for CeCC, a fast stabilization of the oxide resistance at a low value is detected as well as an increase in outer conversion layer resistance. It can be linked to a quick decrease in OCP (Fig. 7 e). CeCC may undergo early corrosion attack due to porosity that induces fast aggressive

Table 2
Resistance, capacitance and *n* parameter evolution during exposure from t_{0+5h} to t_{0+245h} in 0.1 mol/L Na_2SO_4/10^{-3} mol/L NaCl for TCC.

		t0 + 5 h	t0 + 24 h	t0 + 48 h	t0 + 96 h	t0 + 245 h
		Model a)			Model b)	
$R_{electrolyte}$	($\Omega \cdot cm^2$)	39.8	30.4	37.0	33.5	29.6
$R_{conversion:\ outer}$	($\Omega \cdot cm^2$)	107.7	92.4	113.2	–	–
$CPE_{conversion:\ outer}$	($\times 10^{-6}$ $F/cm^2 \cdot S^n$)	2.8	3.3	3.4	–	–
$n_{conversion:\ outer}$		0.78	0.77	0.77	–	–
$R_{conversion:\ inner}$	($\Omega \cdot cm^2$)	2426.0	1350.1	1333.8	–	–
$CPE_{conversion:\ inner}$	($\times 10^{-6}$ $F/cm^2 \cdot S^n$)	0.59	1.3	1.0	–	–
$n_{conversion:\ inner}$		0.93	0.87	0.90	–	–
$R_{conversion}$	($\Omega \cdot cm^2$)	–	–	–	425.8	154.5
$CPE_{conversion}$	($\times 10^{-6}$ $F/cm^2 \cdot S^n$)	–	–	–	30.4	275.8
$n_{conversion}$		–	–	–	0.61	0.41
$R_{corrosion\ p}$	($\times 10^5\ \Omega \cdot cm^2$)	–	–	–	3.7	2.6
$CPE_{corrosion\ p}$	($\times 10^{-6}$ $F/cm^2 \cdot S^n$)	–	–	–	18.2	12.9
$n_{corrosion\ p}$		–	–	–	0.89	0.81
$R_{interfacial\ oxide}$	($\times 10^5\ \Omega \cdot cm^2$)	62.1	14.6	10.0	2.0	0.5
$CPE_{interfacial\ oxide}$	($\times 10^{-6}$ $F/cm^2 \cdot S^n$)	3.0	4.1	4.9	8.5	23.3
$n_{interfacial\ oxide}$		0.92	0.88	0.87	0.89	0.96

species diffusion in the system. An increase of interfacial oxide capacitance (probably convoluted with this corrosion process) (Table 4) is linked to this phenomenon with the appearance of charge transfer phenomenon at the expense of the oxide layer resistance. Moreover, there is a decrease of *n* value of CeCC outer conversion layer close to 0.5 (Table 4). It points out the formation of porous and non protective corrosion products typical of diffusion process [32]. Thus, the RC elements corresponding to $R_{conversion}$ and $CPE_{conversion}$ underline two phenomena that are the barrier effect of the conversion layer and the presence of corrosion product with similar resistance as the conversion resistance. There is a partial compensation of corrosion degradation by continuous formation of the corrosion products even if these products are poorly protective. This results in the limitation of the degradation. Unlike this, as seen previously, WCC presents large cracks that cannot be clogged by corrosion products. As for TCC, the curves from fitting of WCC and CeCC are presented in Fig. 7 d and f.

A mechanism is proposed in Fig. 9 concerning conversion layer evolution during exposure for all the systems. First, for the three systems, there is a modification in the conversion layers: the initially electrochemically distinguishable inner and outer layers evolve towards a single behavior layer with a composition gradient in the thickness (Fig. 9 b, d, f). Concerning TCC, the inner layer is continuous at t_0 and leads to a best barrier effect that seems to be able to inhibit corrosion phenomenon (Fig. 9 a). Presence of protective corrosion products enhances the coating resistance in terms of morphology. The two other systems are different from the TCC. The inner layer of WCC is discontinuous and leads to crack formation during exposure (Fig. 9 c, d). Presence of cracks is an easy way for aggressive ions to diffuse and corrosion process takes place on the substrate. CeCC evolution is similar to WCC because the inner layer of CeCC presents pores close to the inner/outer interface and is then not homogeneous in thickness (Fig. 9 e). Indeed, a thinning of the inner layer at some places due to presence of pores generates a lack of barrier effect, it is supposed that pitting corrosion starts close to these areas (Fig. 9 f). For CeCC, cerium based corrosion products form in pits, which stabilizes the degradation rate contrary to WCC. To summarize, in this hypothesis, the low resistance of WCC and CeCC is mainly due to some defects in the inner layer. The inner layer plays a role of barrier with higher global resistance and *n* values than outer layer. This last one can be rather considered as a supply that stores and provides corrosion inhibitor.

Finally, the use of EIS fitting analysis in combination with morphology characterization allows the understanding of such systems under NSS exposure. Indeed, on the contrary to WCC and CeCC, TCC presents a continuous inner layer at the beginning of exposure. The degradation of this chromium based conversion coating leads to the formation of a more protective corrosion product during exposure. The coupled barrier and self healing effects explain the better performances of TCC under NSS exposure.

4. Conclusion

The issue addressed in this paper is related to the study of the performances as corrosion protective layers of Cr(III) systems compared to alternative ones such as Ce(III) or WO_4^{2-} based conversion systems. The durability of the coatings is studied in a weakly aggressive electrolyte composed of 0.1 mol/L Na_2SO_4 and 10^{-3} mol/L NaCl. The use of both microscopic analyses and electrochemical impedance spectroscopy (EIS), with the help of equivalent electric circuit fitting, is original and allows to understand the influence of the different layers (interfacial, conversion, conversion products) on the degradation phenomena. Even if the Cr(III) based system (TCC) still remains the most durable coating, particularly under NSS exposure, Ce(III) based and WO_4^{2-} based conversion systems (CeCC and WCC) show some promising features.

For Cr(III) conversion coatings, the analysis shows an evolution of

Table 3
Resistance, capacitance and *n* parameter evolution during exposure from t_{0+5h} to t_{0+245h} in 0.1 mol/L Na_2SO_4/10^{-3} mol/L NaCl for WCC.

		t0 + 5 h	t0 + 24 h	t0 + 48 h	t0 + 96 h	t0 + 245 h
		Model c)				
$R_{electrolyte}$	($\Omega \cdot cm^2$)	42.3	40.5	43.6	40.2	39.6
$R_{conversion}$	($\Omega \cdot cm^2$)	160.7	181.5	136.1	172.8	141.2
$CPE_{conversion}$	($\times 10^{-6}$ $F/cm^2 \cdot S^n$)	24.7	44.2	154.3	124.6	275.8
$n_{conversion}$		0.67	0.68	0.65	0.58	0.64
$R_{interfacial\ oxide}$	($\times 10^5\ \Omega \cdot cm^2$)	30.3	5.7	2.8	1.2	0.4
$CPE_{interfacial\ oxide}$	($\times 10^{-6}$ $F/cm^2 \cdot S^n$)	4.2	5.2	7.3	11.4	32.6
$n_{interfacial\ oxide}$		0.93	0.93	0.91	0.91	0.86

Table 4
Resistance, capacitance and *n* parameter evolution during exposure from t_{0+5h} to t_{0+245h} in 0.1 mol/L Na_2SO_4/10^{-3} mol/L NaCl for CeCC.

		t0 + 5 h	t0 + 24 h	t0 + 48 h	t0 + 96 h	t0 + 245 h
		Model c)				
$R_{electrolyte}$	($\Omega \cdot cm^2$)	40.7	33.7	39.0	38.0	39.5
$R_{conversion}$	($\Omega \cdot cm^2$)	251.3	127.5	217.1	493.5	1262.5
$CPE_{conversion}$	($\times 10^{-6}$ $F/cm^2 \cdot S^n$)	57.5	183.5	183.5	251.7	293.3
$n_{conversion}$		0.53	0.46	0.47	0.46	0.47
$R_{interfacial\ oxide}$	($\times 10^5$ $\Omega \cdot cm^2$)	3.4	1.1	1.4	1.2	1.5
$CPE_{interfacial\ oxide}$	($\times 10^{-6}$ $F/cm^2 \cdot S^n$)	4.4	20.9	25.9	33.5	50.6
$n_{interfacial\ oxide}$		0.90	0.91	0.90	0.87	0.81

the microstructure with increasing exposure durations with corrosion products detected all over the sample surface by SEM and also corre lated with the appearance of an additional resistance by EIS. Indeed, in the conditions of the test, corrosion produces protective corrosion products by a self healing phenomenon in the conversion layer.

At the same time, the interfacial oxide resistance decreases. This interfacial resistance can be assimilated to the native oxide formed after the surface preparation. For non corroded samples this resistance is in the range of 10^6 $\Omega \cdot cm^2$ (global resistance after 30 min of exposure), as expected it is similar for the three systems. Once corrosion occurs, the

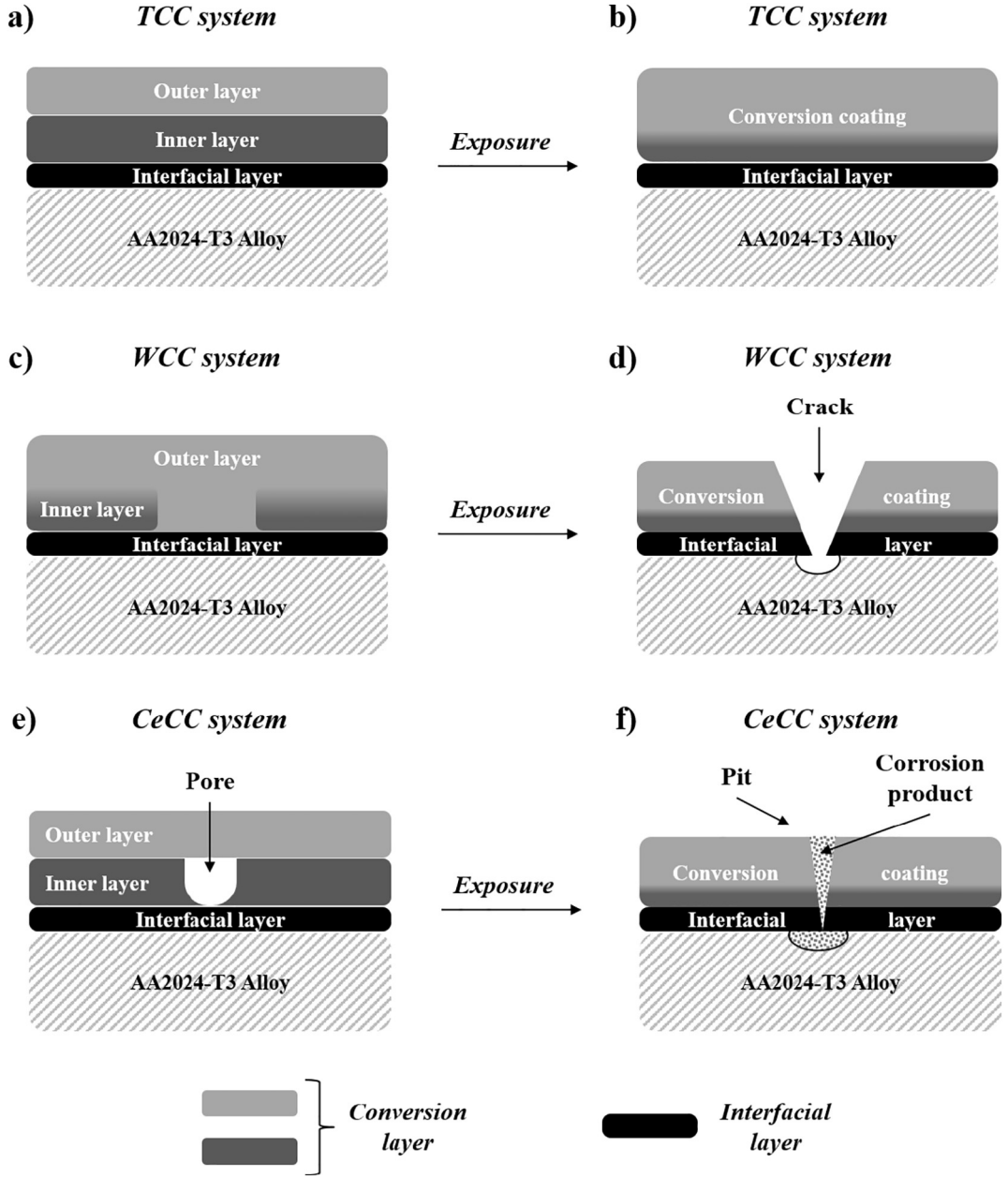

Fig. 9. Schematic representation of (a, b) TCC, (c, d) WCC and (e, f) CeCC evolution after 245 h of exposure in 0.1 mol/L of Na_2SO_4 with 10^{-3} mol/L of NaCl.

resistance of this interfacial layer decreases for all the systems, however a much faster degradation is observed for CeCC.

The conversion layer resistances are in the range 10^2 10^3 $\Omega{\cdot}cm^2$, it remains nearly constant during exposure for all the systems. The highest conversion layer resistances are measured for TCC conversion coatings which is in accordance with their higher thicknesses (150 nm for TCC versus 70 nm for CeCC and WCC).

Two different types of degradation are observed depending on the system: a localized degradation with localized cracks for WCC (corre lated to the presence of localized defects in the inner layer), and a generalized degradation for CeCC (correlated with the presence of pores all along inner layer). So that whereas WCC and CeCC thickness could be increased to reach the thickness value of TCC, this study reveals that a special care should be dedicated to the inner layer morphology of such conversion coatings, the presence of cracks and pores in this layer being the privileged place for interfacial oxide layer attacks and sub sequent substrate degradation.

For TCC systems, it has been proved that performance is not only enhanced by its nature but also by its thickness and its bilayered ar chitecture with: i) an outer layer exhibiting some small pores and ii) an inner compact and continuous layer that works out as a barrier towards the interfacial layer and the substrate.

To sum up, this study gives a new insight and other prospects on the research axis relative to the optimization of chromium free conversion coatings.

Funding sources

This work was supported by the French Ministry of Economy and Industry (BPI France), the Région Occitanie/Pyrénées Méditerranée and the European Union (FEDER/ERDF) in the frame of NEPAL FUI project (AAP FUI n°19).

Acknowledgement

We acknowledge Claudie Josse for FIB observations and Armel Descamps Mandine for ARM analyses.

References

[1] R.L. Twite, G.P. Bierwagen, Review of alternatives to chromate for corrosion protection of aluminum aerospace alloys, Prog. Org. Coat. 33 (1998) 91–100.
[2] B.R.W. Hinton, Corrosion prevention and chromates: the end of an era? Met. Finish. 89 (1991) 15–20.
[3] European Chemical Agency, REACh Annex XIV, https://echa.europa.eu/reach/, (2018) , Accessed date: 4 July 2018.
[4] B.R.W. Hinton, Corrosion inhibition with rare earth metal salts, J. Alloys Compd. 180 (1992) 15–25.
[5] X. Lin, An Environmentaly Compliant Cerium-based Conversion Coating for Aluminum Protection (Ph.D Thesis), University of Missouri-Rolla, 1998.
[6] A.S. Hamdy, A.M. Beccaria, P. Traverso, Corrosion protection of aluminium metal-matrix composites by cerium conversion coatings, Surf. Interface Anal. 34 (2002) 171–175.
[7] B. Rivera, B. Johnson, M. O'Keefe, W. Fahrenholtz, Deposition and characterization of cerium oxide conversion coatings on aluminum alloy 7075-T6, Surf. Coat. Technol. 176 (2004) 349–356.
[8] A. Decroly, J.-P. Petitjean, Study of the deposition of cerium oxide by conversion on to aluminium alloys, Surf. Coat. Technol. 194 (2005) 1–9.
[9] C. Lin, S. Maddela, W.G. Fahrenholtz, M.J. O'Keefe, Deposition of cerium-based conversion coatings on aluminum alloy 380, Int. J. Corros. 2012 (2012) 1–9.
[10] C.E. Castano, M.J. O'Keefe, W.G. Fahrenholtz, Cerium-based oxide coatings, Curr. Opin. Solid State Mater. Sci. 19 (2015) 69–76.
[11] L. Yang, J. Li, C. Lin, M. Zhang, J. Wu, Study of molybdenum/lanthanum-based composite conversion coatings on AZ31 magnesium alloy, Appl. Surf. Sci. 257 (2011) 2838–2842.
[12] A. Losch, J.W. Schultze, H.-D. Speckmann, A new electrochemical method for the determination of the free surface of phosphate layers, Appl. Surf. Sci. 52 (1991) 29–38.
[13] C.G. da Silva, A.N. Correia, P. de Lima-Neto, I.C.P. Margarit, O.R. Mattos, Study of conversion coatings obtained from tungstate-phosphoric acid solutions, Corros. Sci. 47 (2005) 709–722.
[14] T.S.N.S. Narayanan, Surface pretreatment by phosphate conversion coatings - a review, Rev. Adv. Mater. Sci. 9 (2005) 130–177.
[15] D. Rodriguez, R. Misra, D. Chidambaram, Molybdate-based conversion coatings for aluminum alloys. Part II: coating chemistry, ECS Trans. 45 (2013) 1–12.
[16] A.A.O. Magalhães, I.C.P. Margarit, O.R. Mattos, Molybdate conversion coatings on zinc surfaces, J. Electroanal. Chem. 572 (2004) 433–440.
[17] Y. Liu, Z. Li, K. Peng, Preparation method of tungstate conversion film on surface of aluminum alloy, Patent CN101525746 A, 2009.
[18] M.R. Jaworowski, M.A. Kryzman, Compound, non-chromium conversion coatings for aluminum alloys, Patent US6613390B2, 2002.
[19] P. Bares, C. Stephan, C. Gazeau, Method for the surface treatment of parts made of an aluminum of magnesium alloy, Patent WO2013117767A1, 2013.
[20] S.Z. El Abedin, Role of chromate, molybdate and tungstate anions on the inhibition of aluminium in chloride solutions, J. Appl. Electrochem. 31 (2001) 711–718.
[21] M. Fernandez-Garcia, A. Martinez-Arias, J.C. Hanson, J.A. Rodriguez, Nanostructured oxides in chemistry: characterization and properties, Chem. Rev. 104 (2004) 4063–4104.
[22] M. Bethencourt, F.J. Botana, J.J. Calvino, M. Marcos, M.A. Rodríguez-Chacón, Y. Tong, S. Bohm, M. Song, T.N. Zhou, X.D. Qi, Q. Fu, Lanthanide compounds as environmentally-friendly corrosion inhibitors of aluminium alloys: a review, Corros. Sci. 40 (1998) 1803–1819.
[23] G. Boisier, Nouvelles Voies d'Inhibition de la Corrosion de l'Alliage d'Aluminium 2024 plus Respectueuses de l'Environnement: Applications aux Couches d'Anodisation Colmatées (Ph.D Thesis), Université de Toulouse, 2008.
[24] L. Li, Corrosion Protection Provided by Trivalent Chromium Process Conversion Coatings on Aluminum Alloys (Ph.D Thesis), Michigan State University, 2013.
[25] P. Campestrini, E.P.M. Van Westing, J.H.W. de Wit, Influence of surface preparation on performance of chromate conversion coatings on Alclad 2024 aluminium alloy, Electrochim. Acta 46 (2001) 2631–2647.
[26] L. Li, G.P. Swain, A. Howell, D. Woodbury, G.M. Swain, The formation, structure, electrochemical properties and stability of trivalent chrome process (TCP) coatings on AA2024, J. Electrochem. Soc. 158 (2011) 274–283.
[27] M. Kendig, S. Jeanjaquet, R. Addison, J. Waldrop, Role of hexavalent chromium in the inhibition of corrosion of aluminum alloys, Surf. Coat. Technol. 140 (2001) 58–66.
[28] F.W. Lytle, R.B. Greegor, G.L. Bibbins, K.Y. Blohowiak, R.E. Smith, G.D. Tuss, An investigation of the structure and chemistry of a chromium-conversion surface layer on aluminum, Corros. Sci. 37 (1995) 349–369.
[29] D. Ende, W. Kessler, D. Oelkrug, R. Fuchs, Characterization of chromate-phosphate conversion layers on Al-alloys by electrochemical impedance spectroscopy (EIS) and optical measurements, Electrochim. Acta 38 (1993) 2577–2580.
[30] G. Goeminne, H. Terryn, J. Vereecken, Characterisation of conversion layers on aluminium by means of electrochemical impedance spectroscopy, Electrochim. Acta 40 (1995) 479–486.
[31] G.M. Treacy, G.D. Wilcox, M.O.W. Richardson, Monitoring the corrosion behaviour of chromate-passivated aluminium alloy 2014 A-T6 by electrochemical impedance spectroscopy during salt fog exposure, Surf. Coat. Technol. 114 (1999) 260–268.
[32] P. Campestrini, E.P.M. Van Westing, J.H.W. de Wit, Influence of surface preparation on performance of chromate conversion coatings on Alclad 2024 aluminium alloy. Part II: EIS investigation, Electrochim. Acta 46 (2001) 2631–2647.
[33] M. Dabalà, L. Armelao, A. Buchberger, I. Calliari, Cerium-based conversion layers on aluminum alloys, Appl. Surf. Sci. 172 (2001) 312–322.
[34] L.E.M. Palomino, J.F.W. De Castro, I.V. Aoki, H.G. De Melo, Microstructural and electrochemical characterization of environmentally friendly conversion layers on aluminium alloys, J. Braz. Chem. Soc. 14 (2003) 651–659.
[35] L.E.M.M. Palomino, I.V. Aoki, H.G. de Melo, Microstructural and electrochemical characterization of Ce conversion layers formed on Al alloy 2024-T3 covered with Cu-rich smut, Electrochim. Acta 51 (2006) 5943–5953.
[36] J. Qi, Trivalent Chromium Conversion Coatings on Al and Al-Cu Alloys (Ph.D Thesis), University of Manchester, 2015.
[37] Y. Guo, G.S. Frankel, Characterization of trivalent chromium process coating on AA2024-T3, Surf. Coat. Technol. 206 (2012) 3895–3902.
[38] M. Ely, J. Światowska, A. Seyeux, S. Zanna, P. Marcus, Role of post-treatment in improved corrosion behavior of trivalent chromium protection (TCP) coating deposited on aluminum alloy 2024-T3, J. Electrochem. Soc. 164 (2017) C276–C284.
[39] D. Chidambaram, C.R. Clayton, G.P. Halada, The role of hexafluorozirconate in the formation of chromate conversion coatings on aluminum alloys, Electrochim. Acta 51 (2006) 2862–2871.
[40] W.J. Prieto Yespica, Etude Comparative du Comportement Electrochimique des Alliages d'Aluminium 2024 T351 et 7075 T7351 en Milieu Neutre de Sulfate de Sodium (Ph.D Thesis), Université de Toulouse, 2012.
[41] L. Li, K.P. Doran, G.M. Swain, Electrochemical characterization of TCP coatings on aluminium alloys 6061 and 7075, J. Electrochem. Soc. 160 (2013) C396–C401.
[42] L. Li, G.M. Swain, Effects of aging temperature and time on the corrosion protection provided by trivalent chromium process coatings on AA2024-T3, ACS Appl. Mater. Interfaces 5 (2013) 7923–7930.
[43] M.L. Zheludkevich, R. Serra, M.F. Montemor, K.A. Yasakau, I.M.M. Salvado, M.G.S. Ferreira, Nanostructured sol-gel coatings doped with cerium nitrate as pre-treatments for AA2024-T3 corrosion protection performance, Electrochim. Acta 51 (2005) 208–217.
[44] M. Schem, T. Schmidt, J. Gerwann, M. Wittmar, M. Veith, G.E. Thompson, I.S. Molchan, T. Hashimoto, P. Skeldon, A.R. Phani, S. Santucci, M.L. Zheludkevich,

CeO2-filled sol-gel coatings for corrosion protection of AA2024-T3 aluminium alloy, Corros. Sci. 51 (2009) 2304–2315.
[45] D. Borisova, D.G. Shchukin, Influence of embedded nanocontainers on the efficiency of active anticorrosive coatings for aluminum alloys. Part I: influence of nanocontainer concentration, ACS Appl. Mater. Interface. 5 (2013) 80–87.
[46] A. Perrotta, S.J. García, J.J. Michels, A.M. Andringa, M. Creatore, Analysis of nanoporosity in moisture permeation barrier layers by electrochemical impedance spectroscopy, ACS Appl. Mater. Interfaces 7 (2015) 15968–15977.
[47] G.M. Brown, K. Shimizu, K. Kobayashi, G.E. Thompson, G.C. Wood, The growth of chromate conversion coatings on high purity aluminium, Corros. Sci. 34 (1993) 1045–1054.
[48] A.J. Bard, L.R. Faulkner, Electrochemical Methods, 1st ed., John Wiley & Son, Inc., 2000.
[49] M.E. Orazem, B. Tribollet, Electrochemical Impedance Spectroscopy, 2nd ed., John Wiley & Sons, Inc., 2017.